# Development of Ceramic Materials from Mining Waste for the Production of Sustainable Construction Materials

María Paz Sáez-Pérez[1*], Jorge A. Durán Suárez[2]

[1*] Advanced Technical School for Building Engineering Campus Fuentenueva. Avda. Severo Ochoa s/n. 18071 Granada. Spain, mpsaez@ugr.es. https://orcid.org/0000-0001-9725-1153

[2] Fine Arts Faculty. Campus Aynadamar. C/ Periodista Eugenio Selles, s/n, Chana, 18014 Granada. Spain., giorgio@ugr.es. https://orcid.org/0000-0002-9714-3555

https://doi.org/10.29227/IM-2025-02-02-004

Submission date: *2025-03-31* | Review date: *2025-05-01*

*Abstract*

The construction industry faces a challenge in adopting sustainable practices that minimize environmental impact. The search for eco-friendly alternatives has led to the development of materials incorporating recycled waste, optimizing natural resource use. For that reason, ceramic materials with recycled mining waste are gaining attention for their ability to improve the physical and mechanical properties of products while managing mining waste. This approach aligns with circular economy principles by promoting material reduction, reuse, and recycling, which in turn reduces CO2 emissions and enhances manufacturing sustainability. Innovations in the ceramic industry can play a key role in transitioning to a more environmentally responsible model. In this research the main goal is understand the properties and environmental benefits through efficient waste management in new construction materials. For that, this study develops new ceramic materials using recycled mining sludge from Panasqueira mine (Portugal) exploring their potential for sustainable production. Specifically, this research evaluated the impact of adding different proportions of mining sludge (10%, 25%, and 50% by weight) on ceramic brick manufacturing and the samples were fired at controlled temperatures of 800, 950, and 1100 °C, allowing the evaluation of the thermal influence on the final properties of the samples. The methodology employed involved multiple stages, and the following methods were employed: the chemical and mineralogical properties of the materials used were analyzed using X-ray fluorescence (XRF) and X-ray diffraction (XRD) techniques to identify their composition. TGA was performed to assess the thermal properties of the materials. Elastic properties and compactness were evaluated by measuring ultrasonic pulse velocities. The mineralogy, texture, and microstructure of the samples were examined using SEM, providing detailed information about the structural and compositional characteristics. The chromatic properties get to study the aesthetic effects of waste incorporation and their use in new and ancient buildings. The results highlighted that the addition of mining sludge did not significantly alter the overall mineralogy. However, XRD and SEM analyses confirmed that sludge acted as a flux, promoting the formation of mineral phases at lower temperatures and increasing the vitreous phase, improving ceramic structure. The addition of sludge, combined with higher firing temperatures, enhanced the mechanical properties, as evidenced by increased ultrasonic pulse velocities, indicating greater internal cohesion and strength. Color changes were influenced by waste proportions and firing conditions, with higher temperatures (1100°C) producing the most significant variations compared to control samples. The main conclusions confirm that using mining sludge in ceramic manufacturing offered environmental and economic benefits, including reduced clay extraction and water consumption (by 22% to 50%). This led to a more sustainable process, aligning with the industry's goal to lower the carbon footprint. The addition of mining sludge in ceramic brick production improves production sustainability, reducing the use of raw materials, saving energy, and recycling industrial waste. These findings demonstrate the potential of this new ceramic material as an eco-friendly solution for the construction industry. This research is part of the project PCI2024-153488 funded by MICIU/AEI/ 10.13039/501100011033 and ERDF/EU.

**Keywords:** *ceramic-material, mining waste, sustainable, characterization, building*

## 1. Introduction

The construction sector demands vast amounts of resources and materials, also being the primary source of waste generation in the European Union. According to Eurostat 2020 statistics [1], in 2020, the construction activity was responsible for 37.5% of the total waste generated, followed by those from mining and quarries, which accounted for 23.4%. Together, these sectors account for more than half of the waste produced annually across Europe. Furthermore, there is a direct correlation between material extraction activities, the production of construction goods, and the construction activities themselves, which together contribute between 5% and 12% to global greenhouse gas emissions.

In recent decades, especially through the regulatory framework of the European Union, there has been a growing awareness of environmental sustainability. A notable example of this is the Circular Economy Action Plan [2]. In contrast to previous industrial waste management policies — which generally relied on mass storage, often uncontrolled and hazardous — new strategies have emerged focused on the reduction and reuse of these wastes. Nowadays, they are valued as suitable by-products for the production of innovative materials [3]. This shift has been crucial in optimizing waste management, profitability, and resource utilization across various industrial sectors. One of the main sectors is the mining industry, vital for global economic development, which faces significant environmental challenges, particularly in tailings management. These fine-grain mineral processing wastes, if mishandled, can cause soil and water pollution through acid mine drainage and heavy metal leaching, threatening local ecosystems and water resources [4-7]. In this context, the growing emphasis on sustainable practices and the increasing demand for raw materials has spurred research into the recovery and use of mining waste.

Specifically, the construction industry, a major consumer of raw materials, offers a promising avenue for reusing mining waste [8]. Currently, the search for sustainable alternatives in the construction industry has driven the development of innovative materials incorporating recycled waste, thus reducing environmental impact and optimizing the use of natural resources. Mining waste has been successfully integrated into a wide range of construction materials, as evidenced by various studies [9]. This recovery being its main avenue of reuse [10-13]. With its incorporation, the construction industry faces a crucial challenge, focusing on advancing towards more sustainable practices that reduce environmental impact. Main applications include cemented paste backfill for soil support [14], eco-bricks [15], and geopolymeric concrete [16]. These range from relatively simple applications like using processed waste/tailings as fine aggregate replacements in concrete [17] to more sophisticated approaches like alkali-activated materials [18]. In other cases, research has specifically focused on enhancing the cementitious properties of mining waste through mechanical and chemical activation methods [19,20].

Among these advances, ceramic materials with additions of recycled mining waste have gained increasing interest due to their ability to improve the physical and mechanical properties of ceramic products, while also contributing to the management of mining waste. According to recent research, incorporating these wastes into ceramic materials not only reduces the demand for natural resources but also helps improve certain mechanical and thermal properties of the final products [21]. Furthermore, these advancements align with the principles of the circular economy, promoting the reduction, reuse, and recycling of materials within production cycles [22], reducing CO2 emissions, and improving the sustainability of manufacturing processes [23]. In this way, innovation in the ceramic industry can play a key role in transitioning to a more sustainable and environmentally responsible model.

This study provides an overview of the field and aligns with several United Nations Sustainable Development Goals (SDGs). Specifically, it contributes to SDG 9 by promoting the innovative use of mining waste, to SDG 11 through the development of sustainable construction materials, to SDG 12 by encouraging the reuse of industrial waste, and to SDG 13 by highlighting research that can reduce the carbon footprint in the mining and construction industries. This focus on sustainability and innovation underscores the scientific and social relevance of practical applications in the recovery and use of mining waste in construction. With the aforementioned background, the objective of this work is to develop new ceramic materials from the recycling of mining sludge from the Panasqueira mine (Portugal), demonstrating their feasibility for producing sustainable materials with diverse applications. This study aims to deepen the knowledge of the properties of these ceramic materials and their potential contribution to reducing environmental impact, promoting more efficient management of mining waste.

## 2. Materials and methods

### *2.1. Materials*

The clay material used for the brick production was supplied by Cerámica Castillo Siles S.L., located in Viznar (Granada, Spain). This type of clay is commonly used in the production of ceramic materials due to its high plasticity and suitable properties for firing [24]. On the other hand, the mining sludge used as an additive was sourced from the residual deposits of the Panasqueira mine, located in Cabeço do Pião and Aldeia da Panasqueira in the Beira Interior region, Portugal. It is considered one of the largest in Europe, serving as a critical supply source in the global market. The Panasqueira mines are a significant mining complex situated in the Serra da Estrela, near the Serra do Açor and the Zêzere River. This deposit is known for its extensive production of tungsten and tin, in addition to other minerals such as cassiterite and beryllium, and metals like copper and lead [25, 26].

The ceramic samples consist of a mixture of clay and mining waste sludge incorporated in proportions of 10%, 25%, and 50% by weight. The resulting formulations were classified into the VP10, VP25, and VP50 groups (see Table 1). As a reference, control samples (VC) composed solely of clay were also prepared to analyse the effect of the sludge on the properties of the developed materials.

The preparation of the ceramic pastes began with the dry mixing of the clay material with the mining sludge, followed by the addition of water to achieve the desired plastic consistency. The mixture was then manually homogenised to ensure uniformity. The pieces were shaped using removable molds measuring 16 x 12 x 4 cm. Prior to firing, the samples were dried in a laboratory oven at 60 °C for 24 hours to minimise potential adverse effects associated with rapid drying. They were then fired at controlled temperatures of 800, 950, and 1100 °C to evaluate the thermal influence on the final properties of the samples. The laboratory conditions were Tº = 20°C and RH = 60%.

An electric oven (Herotec model CR-35), with a maximum temperature capacity of 1350 °C, was used for this process. The thermal conditions were consistent for all samples, following the stages outlined below: • Gradual heating from room temperature at an increase rate of 120 °C/h until the maximum specified temperature was reached. • Temperature stabilization for 30 minutes at the predefined levels of 800, 950, or 1100 °C.

• Natural cooling by freely decreasing the temperature until ambient conditions were restored.

A total of 48 samples were prepared, with 12 samples per group. Table 1 includes the designation and dosage of each group.

Tab 1. Denomination and composition of the sample groups

| **Tª (ºC)** | **Control** | **Minig muds (wt%)** | | |
|---|---|---|---|---|
| | | **10 %** | **25 %** | **50 %** |
| 800 | VCR | VP10R | VP25R | VP50R |
| 950 | VCM | VP10M | VP25M | VP50M |
| 1100 | VCE | VP10E | VP25E | VP50E |
| Water (mL) | 300 | 235 | 225 | 150 |

### *2.2. Methods*

***Chemical and Mineralogical Characterization of Raw Materials and Prepared Samples***

The chemical and mineralogical characteristics of the materials used in the samples were analyzed using X-Ray Fluorescence (XRF) and X-Ray Diffraction (XRD) techniques. Prior to preparing the samples, the raw materials were analyzed using XRF. A PANalytical Zetium X-ray fluorescence spectrometer was employed for this, equipped with a ceramic X-ray tube, a 4 kW rhodium anode X-ray generator, and a decoupled θ/2θ goniometer.

Subsequently, for the XRD analysis of the samples, a Bruker D8 Advance diffractometer with a 2θ geometry was used, employing copper radiation and a Lynxeye detector. This equipment, available at the Scientific Instrumentation Centre (CIC) of the University

of Granada, enabled phase composition identification using Xpowder software [27]. The analyses were carried out at the CIC of the University of Granada.

***Thermogravimetry***

The analysis was performed using a Thermo Scientific CHSN TM FlashSmart elemental analyzer. Additionally, the heat capacity was determined using an IKA Werke C5003 calorimeter pump. The grain size of the raw materials was independently evaluated using a Galai CIS-1 laser measurement device. The thermal decomposition of the initial material up to a temperature of 950 °C was analyzed using a METTLER-TOLEDO TGA/DSC1 thermogravimetric analyzer, coupled with a differential scanning calorimeter. For this procedure, the samples were placed in an aluminum crucible and exposed to a constant air flow atmosphere of 50 ml/min. The heating rate was controlled at 20 °C/min, reaching a maximum temperature of 950 °C.

***Properties Evaluated by Ultrasound***

The elastic properties and compactness degree of the samples were determined by measuring the propagation speed of ultrasonic pulses. This analysis was conducted using a Steinkamp BP5 ultrasonic pulse generator, equipped with 100 kHz transducers. The direct transmission technique was used, with an aqueous gel (TELIC, S.A.U.) placed between the sample and the transducers. Twelve samples of each type were tested in three directions before and after subjecting them to thermal treatments. The tests were performed according to standard [28], measuring the propagation of P-waves in m/s.

***Mineralogical and Structural Characterization by SEM***

The mineralogy, texture, and microstructure of the samples were studied using a Zeiss DMS 950 scanning electron microscope (SEM), coupled with a Link QX 2000 microanalysis system at the Scientific Instrumentation Centre of the University of Granada. This technique provided detailed and precise data on the structural and compositional characteristics of the analyzed samples.

***Color***

The chromatic properties of the samples were analyzed using a Konica Minolta CM-2600d/2500d spectrometer. The measurements were performed using the standard CIE D65 illuminant, and the luminosity (L) and chromaticity (a* and b*) coordinates were determined with the help of Spectra Magic software [29]. To ensure the reliability of the results, the evaluations were carried out following the guidelines of standard [30]. Each average value was obtained from five measurements taken at different points on the surface of the samples, ensuring a precise and consistent representation of their chromatic characteristics.

## 3. Results

### *3.1. Chemical and mineralogical characterization of the materials*

The elemental chemical composition of the raw materials used is detailed in Table 2. The materials show a high content of silicon oxide ($SiO_2$), accompanied by significant amounts of aluminum oxide ($Al_2O_3$) and iron oxide ($Fe_2O_3$). Specifically, the clay material is distinguished by containing a high percentage of calcium oxide (CaO), while lower concentrations of magnesium oxide (MgO) and potassium oxide ($K_2O$) are observed in both raw materials.

Additionally, it is noteworthy that the clay has a significantly higher Loss on Ignition (LOI) index compared to the mining sludge, with values of 13.86% and 4.60%, respectively. This suggests a higher amount of volatile materials in the clay, which may influence the final characteristics of the ceramic product during the firing process.

Tab. 2. Chemical composition by XRF analysis (wt %) of raw materials. Data normalized to 100% (LOI-free).

| | **SiO2** | **Al2O3** | **Fe2O3** | **MnO** | **MgO** | **CaO** | **Na2O** | **K2O** | **TiO2** | **P2O5** | **LOI** | **Add** |
|---|---|---|---|---|---|---|---|---|---|---|---|---|
| | (%) | (%) | (%) | (%) | (%) | (%) | (%) | (%) | (%) | (%) | (%) | (%) |
| **Viznar** | 47,46 | 14,77 | 5,55 | 0,07 | 3,78 | 10,11 | 0,67 | 2,58 | 0,77 | 0,12 | 13,86 | 99,74 |
| **Muds** | 57,72 | 13,15 | 11,14 | 0,11 | 1,92 | 0,66 | 0,90 | 2,41 | 0,56 | 0,34 | 4,60 | 93,51 |

The X-ray diffraction (XRD) results for the different ceramic material groups (see Figure 1) reveal a diverse mineralogy in all the evaluated pastes. Quartz was the predominant mineral phase in all the samples, regardless of the percentage of residual material incorporated or the intensity of the thermal treatment applied. Additionally, phyllosilicates, feldspars in a broad sense, plagioclases, and carbonates were identified, with their presence varying according to the firing temperature. Hematites and diopside were also detected in smaller amounts.

For the samples fired at 800°C, mineral phases such as quartz, dehydroxylated illite, carbonates (calcite and dolomite), and orthoclase were observed. At 950°C, no significant mineralogical changes were noted; quartz remained dominant, although the peaks associated with illite decreased without completely disappearing, and carbonates were still present. At this stage, new phases emerged, such as sanidine in the control ceramics (VCM) and albite in the bricks with 50% residual sludge (VP50M), although albite began to develop in the other samples at higher temperatures.

In contrast, bricks subjected to a thermal treatment at 1100°C exhibited significant mineralogical changes. Although quartz continued to be a prominent phase, new mineral phases formed in all the types, such as anorthite and diopside. Notably, mullite appeared exclusively in the ceramics with 25% residual sludge (VP25E), indicating a significant mineralogical transformation at this temperature.

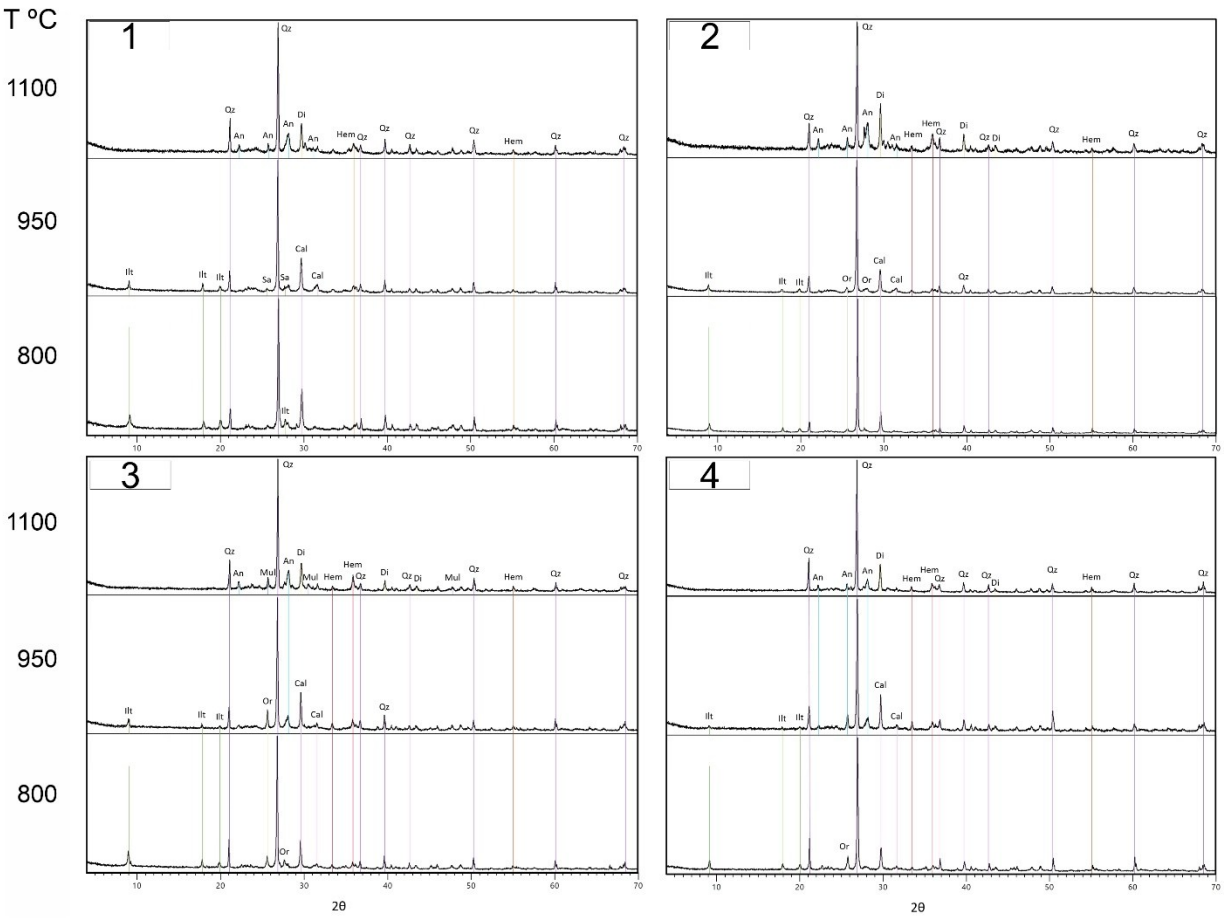


Fig. 1. X-ray diffraction (XRD) analysis of the ceramic pastes (1): VC, (2): VP10, (3): VP25, and (4): VP50 after thermal treatment at 800, 950, and 1100 °C. Legend according to [31]: Qz = quartz; Cal = calcite; Di = diopside; Ab = albite; An = anorthite; Ilt = illite; Sa = sanidine; Hem = hematite; Or = orthoclase; Mul = mullite.

### *3.2. Thermogravimetry*

The results of the differential thermal and thermogravimetric analysis (TG-DTA) of the clay material (Fig. 2) reveal a mass loss of 5% at 98°C, attributed to the evaporation of the hygroscopic water present in the sample [31,32].

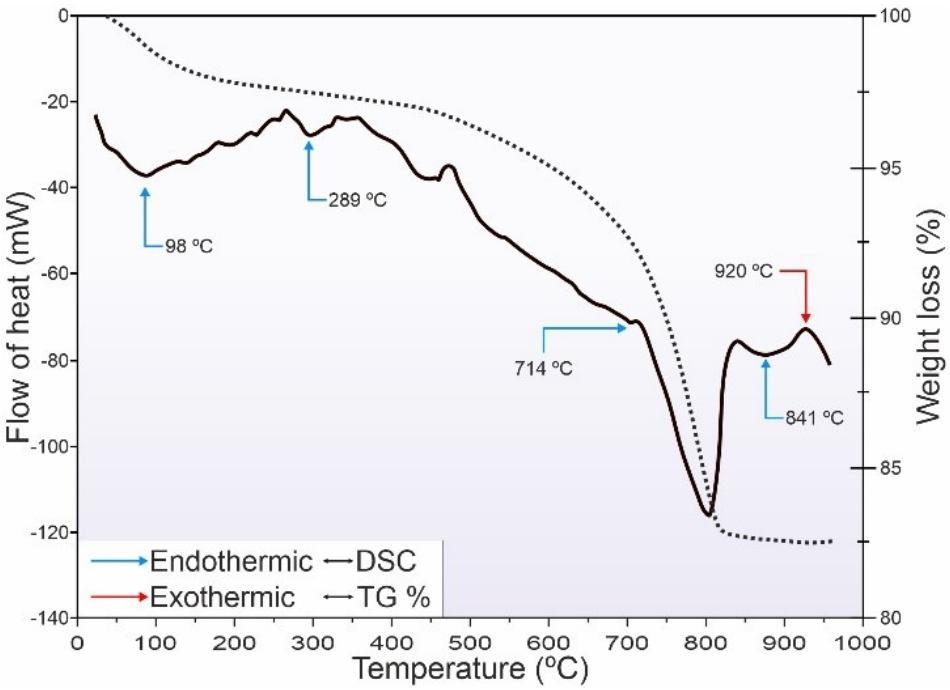


Fig. 2. TG-DSC analysis of the clay material of the samples is represented with the temperature on the x-axis (in ºC) and the y-axes show two different measurements: the right y-axis represents the weight loss (in %) as a function of temperature, while the left y-axis corresponds to the differential scanning calorimetry (DSC) signal (in mW).

The figure shows that at 289°C, there is a curve inflection due to the combustion of residual organic matter, which aligns with [33]. Subsequently, from around 500°C to 714°C, a gradual dehydroxylation of the phyllosilicates occurs, consistent with [34, 35]. During this stage, and up to 800°C, a mass loss of about 15% is observed, matching the loss on ignition (LOI) value identified in the X-ray fluorescence (XRF) analysis. This is attributed to the decomposition of carbonates and the release of $CO_2$, as confirmed by [36].

Additionally, further dehydroxylation of the phyllosilicates present in the sample causes another mass loss starting at 840°C. Finally, at 920°C, an exothermic peak indicates the formation of new crystalline phases [37].

### *3.3. Properties evaluated by ultrasound*

Table 3 provides the average values and standard deviations of the ultrasonic pulse propagation velocities measured across the different brick samples, with ranges spanning from 1214 m/s to 2918 m/s.

Table 3. Average data and standard deviation for the ultrasonic pulse velocity test across the tested sample groups.

Tab. 3. Average data and standard deviation for the ultrasonic pulse velocity test across the tested sample groups.

| Group of samples | Vp (m/s) | σ |
|---|---|---|
| **VC NF** | 1492 | 53 |
| **VCR** | 2019 | 155 |
| **VCM** | 2663 | 66 |
| **VCE** | 2283 | 52 |
| **VP10 NF** | 1481 | 58 |
| **VP10R** | 1214 | 54 |
| **VP10M** | 1895 | 82 |
| **VP10E** | 2276 | 128 |
| **VP25 NF** | 1891 | 109 |
| **VP25R** | 1991 | 189 |
| **VP25M** | 2173 | 35 |
| **VP25E** | 2840 | 57 |
| **VP50 NF** | 1896 | 145 |
| **VP50R** | 1820 | 52 |
| **VP50M** | 2140 | 107 |
| **VP50E** | 2918 | 92 |

In the unfired state, the ceramic pastes containing 25% and 50% of mining sludge (VP25 and VP50) exhibited slightly higher values compared to the control samples (VC) and the formulations with 10% sludge (VP10).

After firing, a progressive increase in ultrasonic pulse propagation velocities is observed as the temperature rises from 800°C to 1100°C, except in the control samples (VC), which reached their maximum velocity of 2663 m/s at 950°C.

Moreover, bricks with higher percentages of mining sludge in their composition showed higher transmission velocities as the additive amount increased. Notably, the VP25E and VP50E groups reached outstanding values of 2840 m/s and 2918 m/s, respectively, after the thermal treatment at 1100°C. These results indicate the formation of a compact and dense ceramic matrix in the samples treated at high temperatures.

According to [38], the temperature increase promotes the formation of crystalline and amorphous phases, leading to higher ceramic density. Simultaneously, the densification of the matrix allows faster propagation of P-waves, thus enhancing the transmission of ultrasonic pulses in the products as the temperature increases.

Graphically, in Figure 3, ultrasonic pulse transmission velocity of the different groups of samples classified by firing temperatures can be observed.

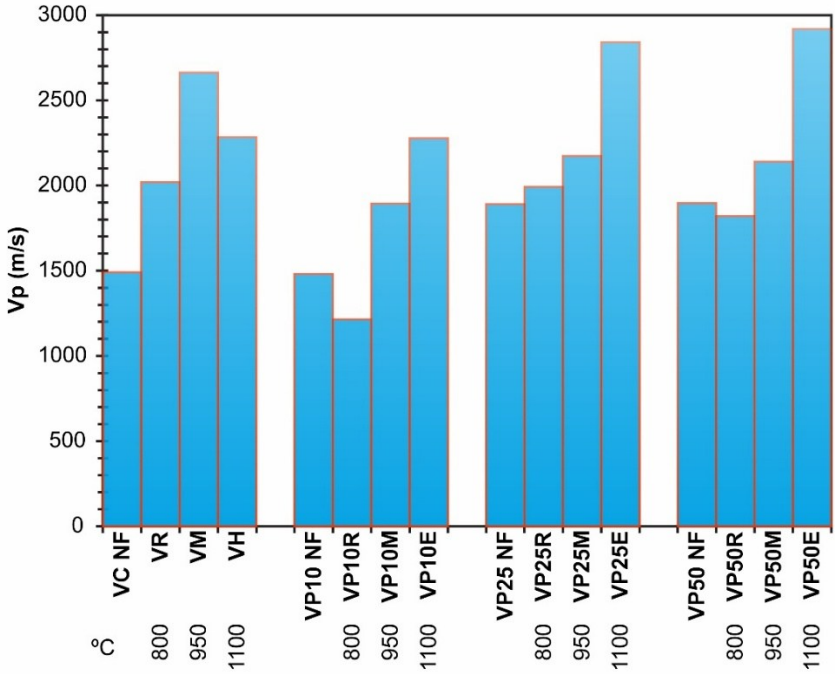


Fig. 3. Ultrasonic pulse transmission velocity of the different groups of samples

### *3.4. Mineralogical and structural characterization by SEM*

The study of ceramic products using Scanning Electron Microscopy (SEM) revealed a complex texture and heterogeneous elemental composition (see Figure 4). Overall, the ceramic matrix is primarily composed of phyllosilicates, with calcium- and potassium-enriched aluminum silicates, as confirmed by X-Ray Fluorescence (XRF) analysis.

Additionally, minerals such as muscovite, a potassium and aluminum silicate with a laminar habit, were identified. Quartz crystals, notable for their size and abundance, were also observed in the raw materials. Complementary observations included calcium and magnesium carbonates, calcium sulfates, and iron recrystallizations, contributing to the mineralogical diversity of the ceramic products.

In ceramic pastes incorporating mining sludge as an additive, additional elements of interest were detected, including arsenic and metals like zinc, titanium, barium, tin, and tungsten. These findings highlight the influence of residual sludge on the composition of the pastes and their potential impact on the final material properties.

The study of ceramic samples fired at different temperatures (800, 950, and 1100 °C) revealed significant changes in texture, morphology, and ceramic matrix characteristics, detailed as follows:

At 800 °C, images 1-4-7-10 show a heterogeneous particle distribution with visible porosity and larger inclusions embedded in the matrix. The texture appears relatively rough, indicating incomplete compaction. This is characteristic of underfired ceramics, with poor consolidation, well-defined mineral grains, and no signs of sintering.

At 950 °C, images 2-5-8-12 still display areas with visible porosity, although reduced in size. A smoother surface is evident, with more noticeable particle contact, hinting at a compact matrix with signs of sintering. Pores retain an angular morphology, and altered carbonate grains due to temperature, along with some shrinkage cracks, are visible.

Significant changes are seen at 1100 °C (images 3-6-9-12). Matrix compaction and vitrification are evident across all types, especially in the pastes containing mining sludge, compared to the control ceramic, where some phyllosilicate layers and unaltered quartz crystals remain visible. The ceramic pastes with 10%, 25%, and 50% sludge exhibit a melted texture, with pores taking on rounded shapes. Gas release and pore closure result in the formation of bubbles.

Overall, these SEM images underscore the heterogeneous nature of the samples, affecting their durability and functional properties.

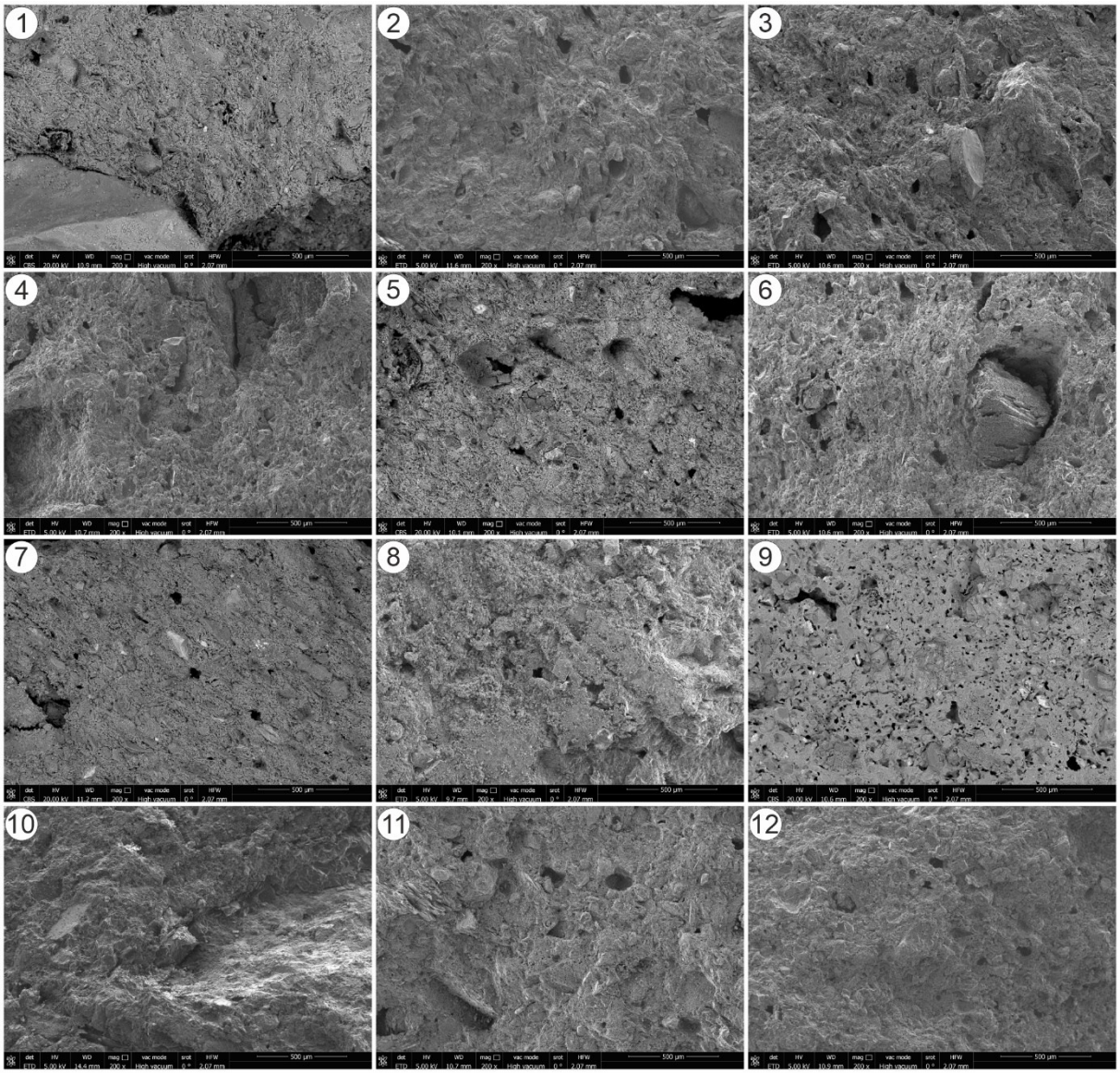


Fig. 4. Representative scanning electron microscopy (SEM). Figures 3.1, 3.2, 3.3: VCR at 800, 950 and 1100 ºC.; Figures 3.4, 3.5, 3.6: VP10 at 800, 950 and 1100 ºC.; Figures 3.7, 3.8, 3.9: VP25 at 800, 950 and 1100 ºC.; Figures 3.10, 3.11, 3.12: VP50 at 800, 950 and 1100 ºC.

The microstructural analysis using SEM confirms the vitrification of the clay bodies mixed with mining sludge. After heat treatment at 1100°C, the ceramics exhibit a molten appearance, along with minerals showing signs of thermal alterations. Finally, both the firing temperature and the amount of residual material added are key factors affecting the color properties of the clay bodies; however, no clear trend based on these variables was observed.

### *3.5. Color*

Table 4 presents the chromatic parameters of the evaluated ceramics. The color of all ceramic products, regardless of the additive percentage or firing temperature, falls within the red-yellow quadrant, characterized by a predominantly orange hue. The bricks show similar dominant wavelength values, ranging from 584 to 588 nm, corresponding to groups VP10E and VP50E, respectively.

Tab. 4. Chromatic parameters of the ceramic products were evaluated using the CIE Lab 1976 color representation system [39] with the D65 illuminant.

| Tª | SAMPLE | λ | | L* | | a* | | b* | | ΔE |
|---|---|---|---|---|---|---|---|---|---|---|
| | | x̄ | σ | x̄ | σ | x̄ | σ | x̄ | σ | |
| 800ºC | VR | 586,18 | 0,37 | 53,11 | 0,31 | 19,31 | 0,92 | 25,44 | 1,00 | - |
| | VP10R | 585,15 | 0,20 | 58,27 | 0,81 | 19,04 | 0,66 | 26,63 | 0,88 | 5,30 |
| | VP25R | 586,90 | 0,22 | 55,68 | 0,32 | 22,59 | 0,50 | 29,33 | 0,46 | 5,70 |
| | VP50R | 585,20 | 0,44 | 53,42 | 1,62 | 19,55 | 0,86 | 28,28 | 0,80 | 2,87 |
| 950ºC | VM | 587,32 | 0,07 | 54,43 | 0,56 | 21,14 | 0,13 | 25,95 | 0,43 | - |
| | VP10M | 586,63 | 0,07 | 56,66 | 0,53 | 20,17 | 0,48 | 25,48 | 0,75 | 2,48 |
| | VP25M | 587,53 | 0,35 | 51,22 | 0,69 | 20,59 | 0,41 | 25,01 | 0,25 | 3,39 |
| | VP50M | 586,97 | 0,33 | 53,28 | 1,41 | 21,03 | 0,41 | 26,71 | 0,48 | 1,38 |
| 1100ºC | VE | 586,09 | 0,30 | 57,54 | 0,73 | 19,62 | 0,47 | 25,61 | 0,46 | - |
| | VP10E | 583,95 | 0,30 | 54,96 | 0,87 | 16,28 | 0,22 | 24,91 | 0,32 | 4,28 |
| | VP25E | 585,33 | 0,96 | 52,54 | 1,04 | 14,64 | 0,63 | 19,12 | 0,45 | 9,59 |
| | VP50E | 588,32 | 0,09 | 49,15 | 1,17 | 19,64 | 0,32 | 22,20 | 0,45 | 9,06 |

Legend: λ (dominant wavelength); L* (lightness from 0 to 100); a* (hue component from red + to green -); b* (hue component from yellow + to blue -); ΔE (total color variation); x̄ (average value); σ (standard deviation).

Although general colorimetric homogeneity is observed, some significant variations stand out. The VP10 group exhibits the highest lightness values, though these decrease as the firing temperature increases. In contrast, the control ceramics (VC group) show an increase in lightness with higher temperatures. For the pastes containing 25% and 50% mining sludge (VP25 and VP50), no clear relationship between lightness, additive content, and firing temperature is noted, with the lowest lightness value of 49 corresponding to the VP50E group. Overall, sludge-containing pastes display lower lightness values compared to the general average, which is around 54.

Regarding hue, in all groups, the b* chromatic coordinate consistently surpasses the a* coordinate, indicating the predominance of the yellow component in the sample colors. In the VP25 group, both chromatic coordinates decrease as the firing temperature rises, whereas in the VC, VP10, and VP50 groups, no clear trend is observed between hue, additive, and temperature.

Lastly, the color differences between the control samples and those with mining sludge additives range from 1.38 to 9.59 units, indicating significant chromatic variations. These differences increase proportionally with the firing temperature, with the highest values seen in the VP25E and VP50E groups. However, samples fired at 950°C exhibit the smallest color variations compared to the control samples, regardless of the amount of residual material incorporated.

Graphically, in Figure 5, the location of the different groups of samples classified by firing temperatures can be observed.

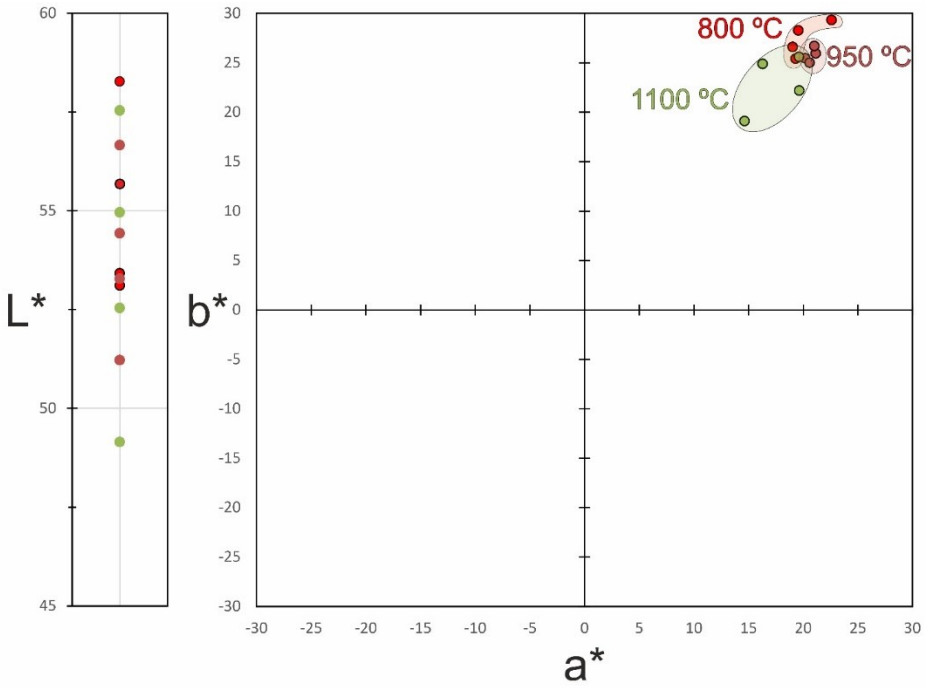


Fig. 5. Graphic representation of the CIELab 1976 [39] values for the different groups of samples with Illuminant D65.

## 4. Conclusions

In this research, the impact of adding different percentages of mining sludge (10%, 25%, and 50% by weight) on the production of ceramic pieces was evaluated. The analyses demonstrated that both the amount of additive and the sintering temperature significantly influence the final properties of the products obtained.

The most relevant conclusions are as follows:

Influence on Mineralogy: The incorporation of mining sludge does not cause significant changes in the overall mineralogy of the ceramics. However, studies using X-ray diffraction (XRD) and scanning electron microscopy (SEM) confirmed that the sludge acts as a flux, facilitating the formation of mineral phases like albite at lower temperatures. Furthermore, it promotes an increase in the vitreous phase, which envelops the minerals, enhancing the ceramic material structure at lower temperatures.

Improvement of Physical-Mecanical Properties: The addition of mining sludge, combined with the increase in firing temperature, improves the mechanical properties of the samples. This was evidenced by the increase in the ultrasonic pulse propagation speeds, suggesting greater internal cohesion and structural strength of the treated samples.

Chromatic Parameters: The color changes in the ceramic pastes were determined by the percentage of mining waste added and the applied thermal conditions. While the predominant wavelength remained constant across all samples, the products fired at 1100°C exhibited the greatest color variations compared to the control samples, highlighting the influence of temperature on the material's aesthetic characteristics.

The use of mining sludge in the production of ceramic materials offers significant environmental and economic benefits. Replacing up to 50% of clay with mining waste not only reduces clay extraction but also lowers water consumption in brick preparation by 22% to 50%. This represents a significant improvement in the sustainability of the process, reducing the demand for natural resources and promoting the recycling of industrial byproducts. Recent studies have shown that reducing clay usage helps to decrease the carbon footprint of the ceramic industry by reducing the volume of material extracted and processed [40]. Additionally, the lower energy demand resulting from the fluxing effect of the additive allows for a reduction in firing temperature, leading to energy savings of up to 15% in ceramic production [41]. The study confirms that adding mining sludge in the manufacturing of ceramic bricks improves production conditions, promoting greater sustainability through reduced use of virgin raw materials, energy savings, and industrial waste recycling. These results strengthen the potential of this new ceramic material as a viable and ecological solution for the construction industry.

To further consolidate the use of mining sludge in the ceramic industry, additional studies are needed, including leaching tests to assess the potential stabilization of harmful elements present in the waste. Furthermore, investigating the performance of the sludge-added ceramic products through accelerated aging tests is recommended to ensure their durability in various environmental conditions.

**Acknowledgments**

This work is part of the action "PCI2024-153488 Project", funded by MICIU/AEI /10.13039/501100011033 and by FEDER, EU, entitled "Valorisation and Integration of Extractive Waste Towards the Sustainability of Raw Materials Industry (ValorWaste)". The authors also want to thank to the Research groups HUM-629 and RNM 0179 (Regional Government of Andalusia).

**References**

1. Alberruche et al., Guía para la rehabilitación de huecos mineros con residuos de construcción y demolición (RCD) (Ministerio para la Transición Ecológica, España, 2018). Available: http://hdl.handle.net/10261/273496
2. Ministerio para la Transición Ecológica y el Reto Demográfico, I plan de acción de Economía circular 2021-2023 Estrategia española de economía circular (MITECO, 2021).
3. Ministerio para la Transición Ecológica y el Reto Demográfico, Estudio ambiental estratégico versión inicial del plan estatal marco de residuos, (Ministerio para la Transición Ecológica y el Reto Demográfico, 2023).
4. M.I. Ahamed and E. Lichtfouse, Water Pollution and Remediation: Heavy Metals (Springer International Publishing, Basingstoke, UK, 2021).
5. E. García-Ordiales et al., "Heavy metal contamination in sediments of an artificial reservoir impacted by long-term mining activity in the Almadén mercury district (Spain)", Environ. Sci. Pollut. Res. 23, 6024–6038 (2016).
6. E.J. Lam et al., "Assessment of the adaptive capacity of plant species in copper mine tailings in arid and semiarid environments", J. Soils Sediments 18, 2203–2216 (2018).
7. E.J. Lam et al., "Methodology to prioritize Chilean tailings selection, according to their potential risks", Int. J. Environ. Res. Public Health 17, 3948 (2020).
8. A. Mehta and R. Siddique, "An overview of geopolymers derived from industrial by-products", Constr. Build. Mater. 127, 183–198 (2016).
9. H.H.M. Darweesh, "Recycling of Glass Waste in Ceramics-Part II: Microstructure of Ceramic Products using XRD, DTA and SEM Techniques", Res. Dev. Mater. Sci. 13 (4), RDMS.000817 (2020). https://doi.org/10.31031/RDMS.2020.13.000817
10. A.N. Ally et al., "Recovery of Mining Wastes in Building Materials: A Review", Open Journal of Civil Engineering 11 (4), 379–397 (2021). https://doi.org/10.4236/ojce.2021.114022
11. N. Cobîrzan et al., "Recycling of mining waste in the production of masonry units", *Materials* **15** (2), 594 (2022). https://doi.org/10.3390/ma15020594
12. T.P. Makhathini et al., "Various options for mining and metallurgical waste in the circular economy: a review", Sustainability 15 (3), 2518 (2023). https://doi.org/10.3390/su15032518
13. S. Saluja et al., "Stabilized municipal solid waste as an alternative to natural sand in paver block construction", Process Safety and Environmental Protection 182, 1035–1046 (2024). https://doi.org/10.1016/j.psep.2023.12.032

14. H. Jiang et al., "Ultrasonic evaluation of strength properties of cemented paste backfill: Effects of mineral admixture and curing temperature", Ultrasonics 100, 105983 (2020).
15. S. Ahmari and L. Zhang, "Production of eco-friendly bricks from copper mine tailings through geopolymerization", Constr. Build. Mater. 29, 323–331 (2012).
16. W.K. Part et al., "An overview on the influence of various factors on the properties of geopolymer concrete derived from industrial by-products", Constr. Build. Mater. 77, 370–395 (2015).
17. A.U. Shettima et al., "Evaluation of iron ore tailings as replacement for fine aggregate in concrete", Constr. Build. Mater. 120, 72–79 (2016).
18. J. Kiventerä et al., "Mine tailings as a raw material in alkali activation: A review", Int. J. Miner. Metall. Mater. 27, 1009–1020 (2020).
19. G. Yao et al., "Activation of hydration properties of iron ore tailings and their application as supplementary cementitious materials in cement", Powder Technol. 360, 863–871 (2020).
20. N. Zhang et al., "Cementitious activity of iron ore tailing and its utilization in cementitious materials, bricks and concrete", Constr. Build. Mater. 288, 123022 (2021).
21. S. Satapathy et al., "Use of mining waste as ceramics and testing for their properties", Sustainable Waste Management Practices for the Mining Sector Through Recycling of Mining Waste, (2024). https://doi.org/10.1007/978-3-031-67932-2_6
22. E. Almeida et al., "A new eco-friendly mass formulation based on industrial mining residues for the manufacture of ceramic tiles", Ceramics International, 2020. https://doi.org/10.1016/j.ceramint.2020.12.260
23. S. Satapathy et al., "Sustainable waste management practices for the mining sector through recycling of mining waste", (2024). https://doi.org/10.1007/978-3-031-67932-2
24. A.G. Porras, "Ceramic production in Granada and in the southeast of the Iberian Peninsula during the late middle ages", Medieval Ceramics 32, 29–43 (2013).
25. A. Franco et al., "The Panasqueira mine at a glance", ITIA Newsletter (2014).
26. E. Carocci et al., "Incipient wolframite deposition at Panasqueira (Portugal): W-rutile and tourmaline compositions as proxies for early fluid composition", Economic Geology 16 (1), 123–146 (2021). https://doi.org/10.5382/econgeo.4783
27. Xpowder software.
28. ASTM D2845-08(2013), Standard Test Method for Laboratory Determination of Pulse Velocities and Ultrasonic Elastic Constants of Rock (ASTM International, West Conshohocken, PA, 2013). Available: www.astm.org
29. Color Data Software CM-S100w. Spectra Magic NX. Version 3.4 (2020).
30. UNE-EN 15886:2011, Conservation of Cultural Property - Test Methods - Colour Measurement of Surfaces (Asociación Española de Normalización (AENOR), 2011).
31. D.L. Whitney and B.W. Evans, "Abbreviations for names of rock-forming minerals", Am. Mineralogist 95, 185–187 (2010). https://doi.org/10.2138/am.2010.3371.185
32. A. Santamaría-López et al., "Geological Setting of Sierra Nevada in the Landscape of the Sierra Nevada", Springer, 71–81 (2022). https://doi.org/10.1007/978-3-030-94219-9_5
33. J. Geng and Q. Sun, "Effects of high temperature treatment on physical-thermal properties of clay", Thermochim. Acta 666, 148–155 (2018). https://doi.org/10.1016/j.tca.2018.06.018
34. N. Touch et al., "Changes in the state of organic matter present in sediment by different methods of electrokinetic treatment", IJERD 10 (1), 47–52 (2019). https://doi.org/10.32115/ijerd.10.1_47
35. M. Achik et al., "Evaluation of technological properties of fired clay bricks containing pyrrhotite ash", Constr. Build. Mater. 269, 121312 (2021). https://doi.org/10.1016/j.conbuildmat.2020.121312
36. L. Heller-Kallai and I. Lapides, "Dehydroxylation of muscovite: study of quenched samples", Phys. Chem. Miner. 42 (10), 835–845 (2015). https://doi.org/10.1007/s00269-015-0767-4
37. T. Hirono and W. Tanikawa, "Implications of the thermal properties and kinetic parameters of dehydroxylation of mica minerals for fault weakening, frictional heating, and earthquake energetics", Earth Planet. Sci. Lett. 307 (1–2), 161–172 (2011). https://doi.org/10.1016/j.epsl.2011.04.042
38. L. Luo et al., "Preparation, characteristics and mechanisms of the composite sintered bricks produced from shale
39. NORMA ISO 11664-2:2007. Colorimetry – Part 2: CIE standard illuminants
40. Q. Gao, S. Simatrang, and E. Joenurairatana, "Research on the Sustainable Utilization of Ceramic Waste under the Green Development Model," E3S Web Conf., 370, 02005 (2023).
41. C. Galhano, P. Lamas, and D. Seixas, "Use of Industrial Waste for the Optimization of Ceramic Construction Materials," in RICON19 - REMINE International Conference on Valorization of Mining and Industrial Wastes into Construction